Article

NOISE & VIBRATION WORLDWIDE

Experimental and numerical investigation of defect-size estimation in taper roller bearing

Noise & Vibration Worldwide
1–10

DOI: 10.1177/0957456518801141
journals.sagepub.com/home/nvw
SAGE

Ahmed Nabhan and Ahmed Rashed

Abstract

In this article, the estimation of different defect sizes present on the outer race of taper roller bearing confirms the effectiveness of the applied method for different vibration signals. Experiments and numerical model conducted for three primary conditions of bearing setting, which are positive, negative, and zero clearance. The outer race is installed in five different positions so that the defect located at 0°, 45°, 90°, 135°, and 180°. The output of the numerical model finds close correlation with the vibration signal pattern–obtained experiments. From the results, it is clear that defect-size estimation is more precise when the defect is introduced in the unloading area, and the contact time depends directly on the size of the defect, through which it is easy to calculate its value of the defect.

Keywords

Vibration analysis, numerical model, defect-size estimation, ABAQUS

Introduction

Tapered roller bearings are anti-friction bearings that have the ability to carry complex loads in both radial and axial directions. Depending on the tapered roller bearing terminology, the bearing may have a small contact angle. This type of bearings is commonly used for high-speed and heavy-duty applications and shafts that require no maintenance for long-term operation. Vibration analysis is among the most widely used methods for detecting bearings defects.[1] Each defect has a distinct vibration behavior, through which the defect can be identified.[2] A linear model was created to give a simulated vibration data. The electrical discharge machining was used to detect the defects of inner and outer race.[3] A finite element (FE) model is built to measure the vibration data for the defected bearing. The measured vibration data for the ideal and defected bearings are compared using the values of the root mean square (RMS).[4,5] A numeric model of the ball bearing is established using ABAQUS to study the effect angular position defect around the outer race. The statistical parameters ratio extracted from simulation through numeric model were used to characterize the bearing performance.[6] Moreover, the model is developed to detect the number of defects on the outer race of the bearing.[7] Spectrum analyses are performed at particular test durations with a view to predict defect locations using the statistical parameters, peak-to-peak value, RMS, crest factor, and kurtosis.[8]

The influence of defect sizes of radial bearings has been studied considering the generated noise.[9,10] An experimental test-rig was utilized such that defects of different sizes have been introduced onto the outer and inner races of a test bearing. The effect of the acting parameters; mainly defect size, running speed, and loading nature; on the generated acoustic emission signals is investigated. Therefore, a modified and effective signal-processing algorithm is introduced to indicate localized defects on rolling bearing components under different operating speeds, loadings, and defect sizes. Results show the superiority of the developed algorithm and its effectiveness in extracting bearing characteristic frequencies.[11] The influence of the inertia and centrifugal forces that affects the rolling elements of a defective anti-friction bearing on the generated vibration signals has been investigated.[12] It is found that, the influence of these effects increases with the increase in the speed of the rolling elements. Furthermore, the analyses presented in this study tend to develop accurate and reliable defect-size estimation algorithms. The dynamic vibration

Production Engineering and Mechanical Design Department, Faculty of Engineering, Minia University, El-Minia, Egypt

Corresponding author:
Ahmed Nabhan, Production Engineering and Mechanical Design Department, Faculty of Engineering, Minia University, El-Minia 61111, Egypt.
Email: a.nabhan@minia.edu.eg

model to study of deep groove ball bearings with localized defects is presented. The vibration signals and frequencies are numerically determined by solving the governing equations of motion.[13] A 5 degree-of-freedom (DOF) model in MATLAB-Simulink environment, a bond graph model, and a numeric model in ADAMS software are developed and validated with experiments.[14,15] Contact stresses of a ball bearing with off-sized balls were investigated. A model has been considered, taking into consideration the stiffness, damping, and friction between the bearing components.[16–18] The output of the model gave the contact deformations between the balls and bearing races, contact forces, and Hertzian contact stresses in each ball. The results show that off-sized balls alter the contact stiffness, contact force and stress concentration in mating bearing surfaces. The stress values are dependent not only on the dimension of the off-sized ball or balls but also their location.

This work is carried out to estimate the defect width in outer race of taper roller bearing using FE model. A three-dimensional (3D) model is established to evaluate a taper roller bearing and to obtain simulated vibration signals of outer-race defect using FE analysis through ABAQUS software. The vibration-monitoring methods are examined using RMS.

Experimental setup

Figure 1 illustrates a schematic of the test rig utilized in the experiments. An asynchronous motor of 0.5 kW capacity with variable speed characteristics up to 6000 r/min is used as power unit. The system allows the adjustment of the shaft rotating speed as well as the direction of rotating through a control unit which is connected to the motor. The main shaft, which is connected to the motor by elastic claw coupling, is supported by two taper roller bearings. The radial load is fulfilled to the tested bearing using V-belt drive pulleys. The bearings have been investigated at five different of speeds, from 1000 to 3000 r/min with steps of 500 r/min at radial loads of 200, 400, and 600 N approximately. The accelerometers (IMI sensors 603C01) are used to collect the signal data of the tested bearing in both vertical and horizontal directions. The vibration signals are acquired using a data acquisition card (BMC USB-AD16F), which are displayed using LabVIEW interface. The software recorded the speed of the shaft by using an electronic reference sensor.

The taper roller bearing SKF 32004 is considered as an object for this study. Figure 2 shows the bearing geometry. Five sets of the defective bearings were investigated, which have 0.46, 0.62, 0.71, 0.84, and 1.05 mm width on the outer race. Figure 3 illustrates different locations of outer-race defects for a bearing which the defect is located at 0º, 45º, 90º, 135º and 180º. Taper roller bearings have a unique feature, cone and cup are separable, which can be set easily and they meet the expected operating conditions.

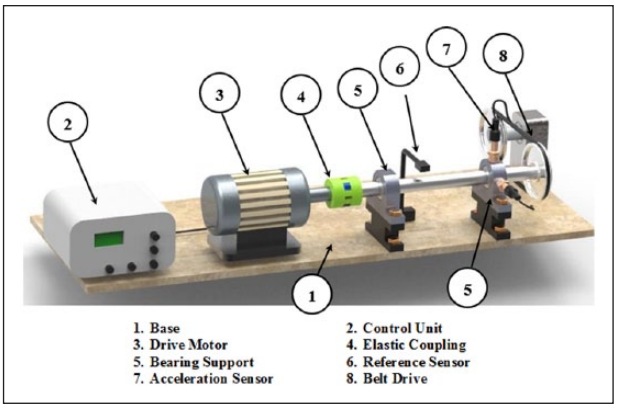

Figure 1. Schematic of the test rig.

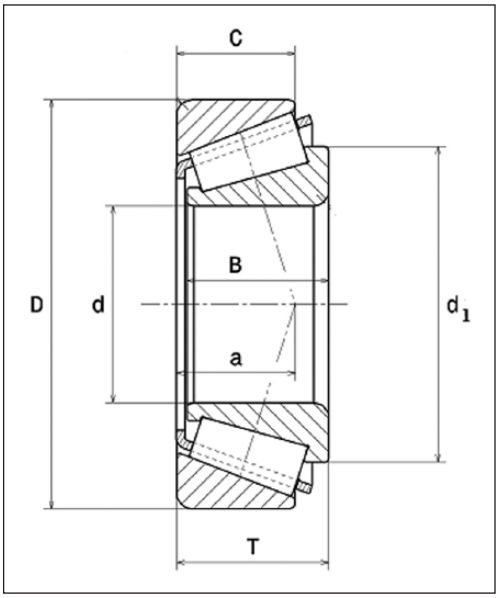

Figure 2. Geometry of the taper roller bearing.

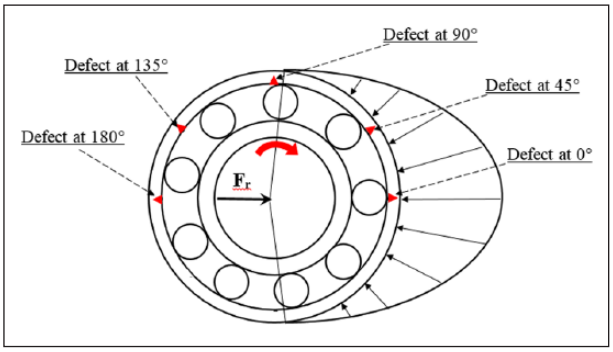

Figure 3. Different locations of outer-race defects for a bearing.

The radial internal clearance can be obtained to determine the required axial drive-up distance. A dial indicator can be positioned at a reference point on the outside surface of the outer race to measure the axial shaft movement. The investigation of the bearing behavior has been carried out for three primary conditions of bearing setting, which are positive clearance, negative clearance, and zero clearance. Positive clearance is obtained when axial clearance between rollers and races produces a measurable axial shaft movement (load zone less than 180°). Zero setting condition is obtained when there is no discernible axial shaft movement (load zone equal to 180°). Negative clearance (i.e. pre-load) is obtained when the dial indicator measures axial clearance on the opposite direction (load zone greater than 180°).

The bearing dimensions and parameters are as follows:

Outer diameter, D = 42 mm	Bore diameter, d = 20 mm
Pitch diameter, d_m = 31 mm	Cup width, C = 12 mm
Bearing width, T = 15 mm	Core width, B = 15 mm
Roller diameter, d_r = 4.86 mm	Contact angle, α = 14.036°
Number of rollers, n = 16	

A mathematical method and numeric model for contact analysis

Contact between the rolling elements and raceways in rolling bearings is considered a two solid elastic cylinders (Figure 4). The mating surfaces held in contact by radial load uniformly distributed along the cylinder length. The Hertzian theory of elastic deformation of contact between elastic bodies can be used to find contact areas and indentation depths for simple geometries.

The half-width of the rectangular contact area of two parallel cylinders

$$a = \sqrt{\frac{2Q\left[\frac{1-\upsilon_1^2}{E_1}+\frac{1-\upsilon_2^2}{E_2}\right]}{\pi L\left(\frac{1}{d_m}+\frac{1}{d_r}\right)}} \quad (1)$$

where E_1, E_2 are the modulus of elasticity for the race and rollers; υ_1, υ_2 are Poisson's ratio for the race and rollers; d_r is the roller diameter; d_m is the pitch diameter; and L is the length of cylinders

$$Q = \frac{4.08 F_r}{n \cos\alpha} \quad (2)$$

where, F_r is the radial load, n is the number of rollers, and α is the contact angle.

The maximum contact pressure along the center line of the rectangular contact area is computed as

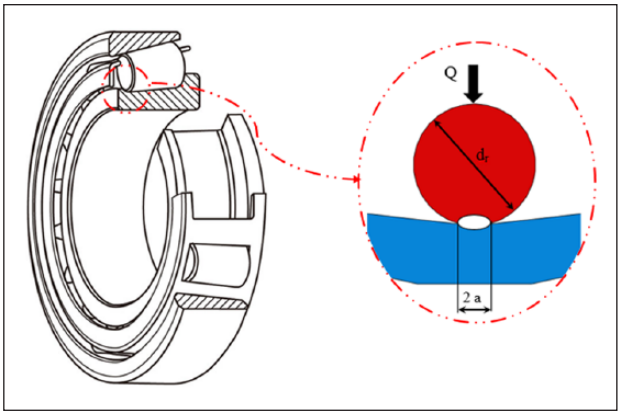

Figure 4. A semi-elliptic pressure distribution across contact over zone of diameter 2a.

$$P_{max} = \frac{2Q}{\pi a L} \quad (3)$$

The principal stresses σ_1, σ_2, and σ_3 are generated on the z-axis

$$\sigma_1 = -2\upsilon P_{max}\left[\sqrt{1+\xi^2} - |\xi|\right] \quad (4)$$

$$\sigma_2 = -P_{max}\left[\left(\frac{1+2\xi^2}{\sqrt{1+\xi^2}}\right) - 2|\xi|\right] \quad (5)$$

$$\sigma_3 = -P_{max}\frac{1}{\sqrt{1+\xi^2}} \quad (6)$$

where $\xi = z/a$ non-dimensional depth below the surface

Numerical model is built as a 3D model to recognize steps of the bearing Hertzian contact analysis. The roller and the race are made of the same material. The material is isotropic and homogeneous steel, with modulus of elasticity of 210 GPa and Poisson's ratio of 0.29. Before contact, analyses of the bearings are performed, and the interaction between surfaces is defined as surface-to-surface contact with no adjustment. The lower surface of the race is developed as fixed part which has no DOF, ENCASTRE, U1 = U2 = U3 = UR1 = UR2 = UR3 = 0. Furthermore, the roller is developed as a part which has 3 DOF, U1 = U3 = UR3 = 0. For analyzing the geometric contact, a 3D model mesh is developed using hexahedron solid element, which has eight nodes with reduced integration and eight nodes (C3D8R). The reduced integration with eight nodes element (C3D8R) has been replaced with fully integrated, eight-node element (C3D8) to ensure high computation accuracy of contact stresses. Figure 5 illustrate the mesh-seed pattern of roller bearing with the fully integrated eight-node element (C3D8).

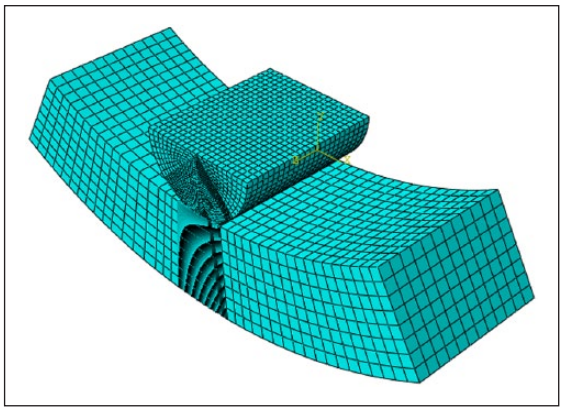

Figure 5. Mesh-seed pattern of the roller bearing.

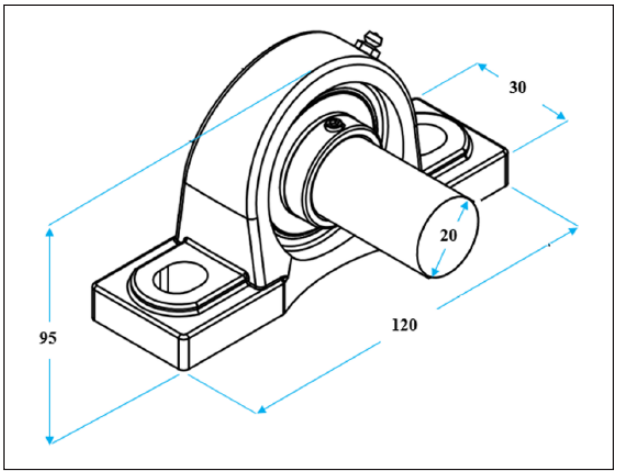

Figure 6. Basic dimensions of the housing structure (dimensions in mm).

A bearing model development for vibration analysis

As a result of anti-friction, bearings are subjected to dynamic uniform radial and axial forces. A convenient model should be developed to analyze vibration response of taper roller bearing using the commercial software ABAQUS. The model has been considered to be with stationary outer race while the inner race was free. Furthermore, it is assumed that the contact between the outer surface of the outer race and its mating surface on the casing structure is ideal, that is, there is no relative motion (slip) permitted on the contact surface. The 3D model of the housing and bearing-outer race is established in commercial package ABAQUS/CAE. The housing model is created according to the dimensions shown in Figure 6. The element type utilized in the mesh is eight nodes with reduced integration (C3D8R). Both housing and race are recognized with the same element type but using uneven global sizes. It is assumed that the bearing material is isotropic steel, and the housing is considered as an isotropic aluminum.

	Elastic modulus, GPa	Poisson's ratio	Density, Kgm^{-3}
Race	210	0.29	7850
Housing	68.9	0.33	2700

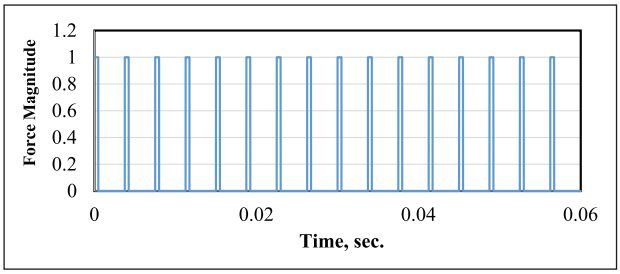

Figure 7. Dynamic loading models for node at 0° acting on a contact area.

Interaction between inner surface of the housing hole and the outer surface of the bearing-outer race are defined as tie constrains. The housing part is developed as fixed part which has no DOF, ENCASTRE, U1 = U2 = U3 = UR 1 = UR2 = UR3 = 0. In the analyzed case, the nodes on the inner surface of the outer race are subjected to different amplitude loads at any instant of rotation. Duration of the impacts is determined by the rotational speed of the shaft. A radial force is defined due to the assumption of the contact area. A sample loading function for the nodes on the inner surface is given in Figure 7 for one rotation of the shaft rotating. The general governing equations of the system are written as

$$[M]\begin{Bmatrix}\ddot{x}\\ \ddot{y}\end{Bmatrix}+[C]\begin{Bmatrix}\dot{x}\\ \dot{y}\end{Bmatrix}+[K]\begin{Bmatrix}x\\ y\end{Bmatrix}=\{f(t)\} \tag{7}$$

where M, C, and K are the mass, damping, and stiffness matrices, respectively; $x, \dot{x}, \ddot{x}, y, \dot{y}, \text{and } \ddot{y}$ are the nodal displacement, velocity, and acceleration vectors in both direction, respectively. The right-hand side of the equation consists of time-dependent excitation functions acting on each DOF of the FE nodes. The bearing structure is excited by a moving distributed radial load on the inner surface of the outer ring. The right-hand side of equation (7) is formed, considering the bearing kinematics and radial-load distribution, and the vibration response of the bearing structure is examined under the different operating conditions.

As a result, the contact is assumed to be a line contact, and the magnitude force acting is estimated as a square form. The contact area can be calculated according to the Hertzian theory, for the elastic deformation of contact between elastic bodies can be used to find elastic contact area for engineering bodies.[19] In the case of taper roller

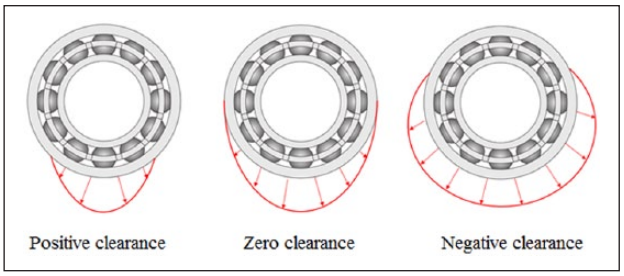

Figure 8. Load distribution for different radial clearance.

bearing, the contact area of two matting is cylinder to cylinder, as shown in Figure 7. Therefore, the half-width of the rectangular contact area of two parallel cylinders is calculated according equation (1). The loads carried by the roller bearings are transmitted through the rolling elements from one race to the other and tend to deflect the bearing races. The load distribution around the circumference of a rolling element bearing under radial load is defined as

$$Q_\psi = Q\left[1-\frac{1}{2\varepsilon}\left(1-\cos\psi\right)\right]^{1.11} \tag{8}$$

where ε denotes the load distribution factor and is given as $\varepsilon = 0.5\left(1-C_d/2\delta_{max}\right)$. C_d denotes the diametral clearance, and δ_{max} denotes the maximum deflection in the direction of radial load.

The investigation of the bearing behavior has been carried out for three primary conditions of bearing setting, which are positive clearance, negative clearance, and zero clearance. In case of positive clearance ($0<\varepsilon<0.5$), the load zone will be less than 180°. If there is no internal clearance ($\varepsilon=0.5$), then one half of circumference of the rollers will be under the acting load while the contact zone "ψ_1" reaches an angle of 180°. For the case of negative clearance or pre-load ($0.5<\varepsilon<1$), the whole circumference is equally loaded and the contact zone "ψ_1" will be near the value of 360°. Figure 8 illustrates the variation of load distribution among the rolling elements for different contact angles "ψ_1".

Figure 9(a) shows the outer-race structure of the bearing which is partitioned into 16 parts. The dynamic excitation of the bearing structure can be established by applying the radial load of equation (8) on each node along the inner circumference of the loading zone. The magnitude of the load carried by a particular rolling element changes as the angle of contact "ψ" changes. The rolling elements which are outside of the loading zone do not carry load, as shown in Figure 9(b).

Normal mode dynamics is used to find dynamic responses at two receiving points. Duration of the impacts is determined by the rotational speed of the shaft. Impact

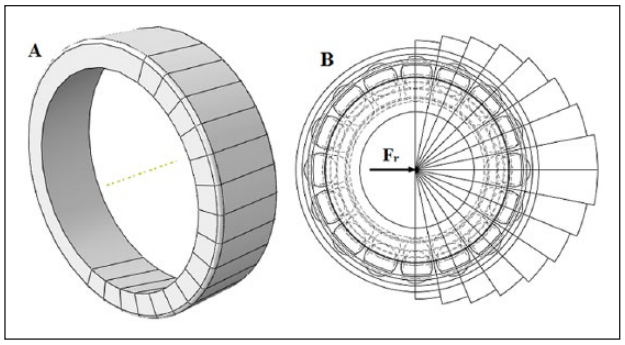

Figure 9. Outer race after partition into 16 parts and the distribution of acting loads.

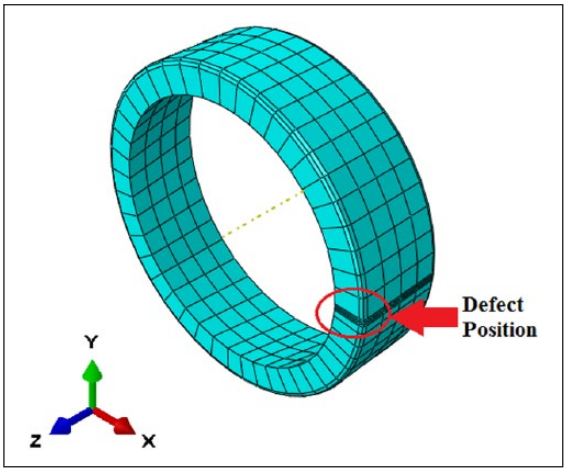

Figure 10. Mesh seed of defected outer race.

duration reduces as the shaft speed increases. The mechanism of defect formation can be different in a rolling element bearing. Sudden changes in the radial load may result a local defect during operation. The magnitude and the duration of the impulse force are related with the radial load carried by the outer-race defect and the velocity of the rolling elements, as shown in Figure 7. A local defect is modeled by amplifying the magnitudes of the radial forces defined for the nodes which are in the defected area, as shown in Figure 10. The amplification constant is chosen simply as 6.775 (equation (9)) in this study. Outer-race defect frequency (defect on outer race)

$$f_o = \frac{nf_s}{2}\left(1-\frac{D}{d_m}\cos\alpha\right) \tag{9}$$

Results and discussion

Hertzian contact analysis

The rectangular contact area of two parallel cylinders is calculated according to certain variable using the Hertzian contact theory. The generated stresses of the roller bearing

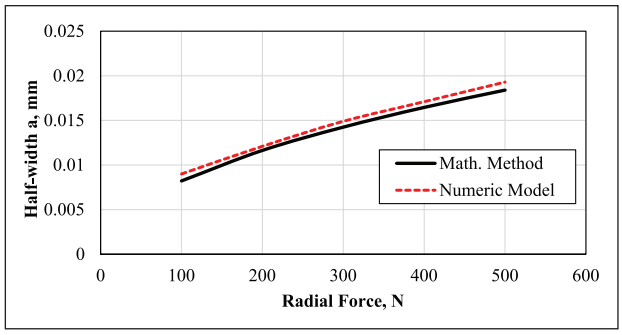

Figure 11. Contact area comparison between the numeric model and Hertzian theory.

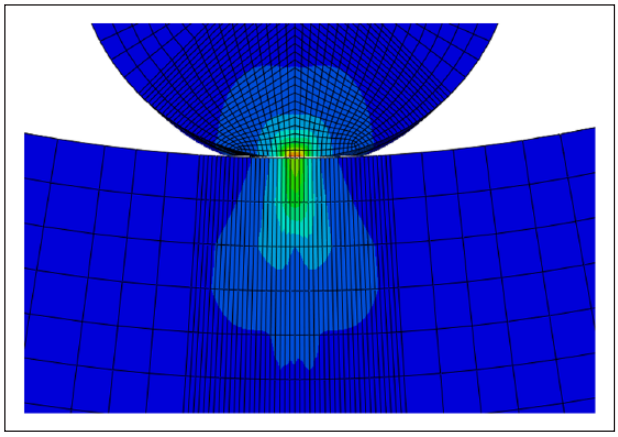

Figure 12. Stresses distributed on the contact surface.

are also calculated according to Hertzian theory. Figure 11 illustrates a comparison of the rectangular contact area between the developed numeric model and Hertzian theory. It is indicated that the width of contact area obtained by the numeric model, illustrated with ABAQUS software, is totally similar to the one calculated using Hertzian theory. Figure 12 shows the contact stress distribution between the roller and the outer race. The radial load is 100 N when the analysis is developed. It can be noticed that the maximum contact stress point is located at the center of the contact area. And the maximum contact stress is extended along the width of the roller and the race, as shown in Figure 13. The stress distribution along the thickness of the race material can be determined using the numeric model. However, the mathematical method cannot be used to calculate the stress distribution due to the effect of the loads at the longitudinal path of the contact area.

Defect-size estimation

The same operating conditions of the process have been chosen to satisfy a suitable symmetry between the experimental tests and the dynamic numeric model. Here, bearing with one defect at 0°, the taper roller bearing used in

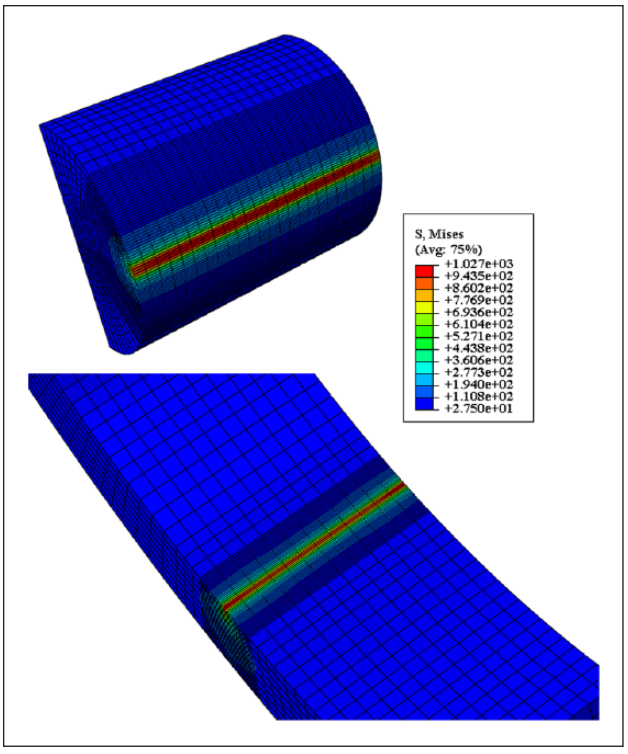

Figure 13. Stresses distributed on the roller and outer race.

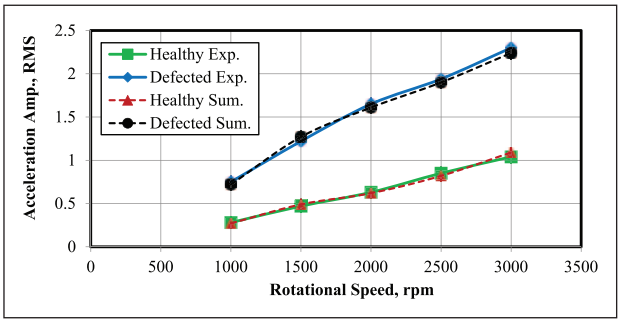

Figure 14. Validation between experimental and simulation results for zero clearance bearing "$\varepsilon = 0.5$".

the experiments and the dynamic model have the same size of defect and were tested at different shaft speeds. Both the experiments and the dynamic model were studied at bearing with zero clearance ($\varepsilon = 0.5$), the action of pure radial load tends to a contact zone between the bearing parts; i.e. rollers, outer and inner race; with angle of action "ψ_1", which ranges from zero to 180°. Validation between the experimental and simulation results illustrates in Figure 14. The variation of the RMS of the amplitude of the acceleration for the healthy bearing and the defected one "RMS" versus the shaft speeds is measured at the horizontal measuring point. It is clear that, the results are a good agreement between both cases. It is concluded that, the variation between the experimental and simulation results is less than 4.8%.

As a result of the knowledge of vibration impact duration Δt which is estimated using vibration signals-based decomposition, shown in Figure 15, the mating surface width is[19]

$$b = \pi D_{ave} \Delta t \, FTF \tag{10}$$

where FTF is the fundamental train frequency, and D_{ave} is the average outer-race inner diameter of the bearing

$$FTF = \frac{f_s}{2\left(1 - \frac{d_m \cos \varnothing}{d_r}\right)} \tag{11}$$

where f_s is the number of revolutions per second

Based on that, the method to determine the size of the outer-race defect by calculating the contact time between the roller elements and the defect is inaccurate. Figure 16 illustrates the acceleration profile of the defected outer race measured at position 1 "θ = 0°" at radial load of 100 N and rotational speed 100 r/min. It can be cleared that the lab interface allows to display the vibration signals with more intensity, through which it can detect defects while not being able to calculate the contact time. Furthermore, the vibration signals are obtained from the dynamic numerical model of the defected outer race measured at position 1 "θ = 0°" and position 3 "θ = 180°", respectively, as shown in Figures 17 and 18. It can be observed that the contact time of case position 1 "loading area" have a higher value than found at position 3 "unloading area". It may be due to the fact that the contact time in the first case depends not only on the size of the defect but also on the loading conditions. It can be concluded that the contact time in the loading area depends on the shaft speed, the radial-load value, type of clearance, and the size of the defect. While in the unloading area, the contact time depends directly on the size of the defect, through which it is easy to calculate its value of the defect. It is also possible through the dynamic model to easily study the vibration response of the anti-friction bearing. Where, it can analyze vibration

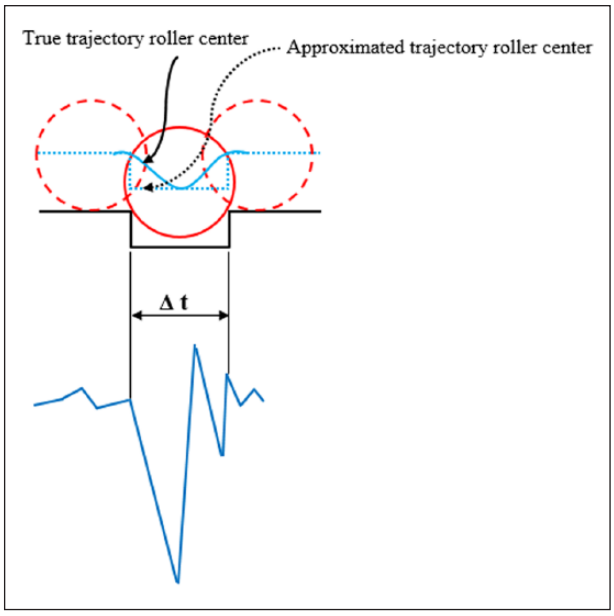

Figure 15. Typical vibration impact duration and the corresponding roller positions over an outer-race defect.

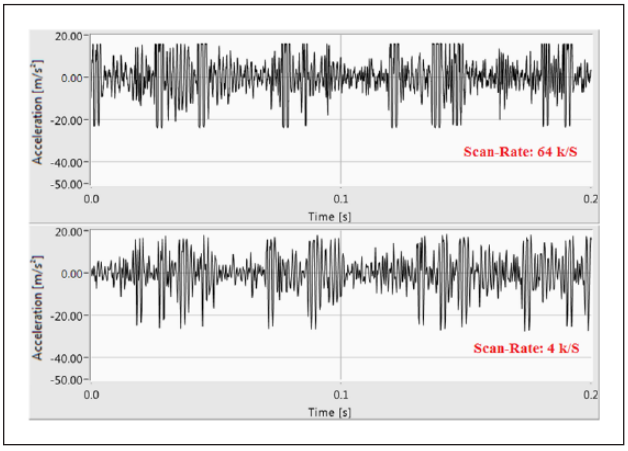

Figure 16. Experimental acceleration response for bearings with defected outer race at position 1 "θ = 0°—defect is located at the load zone".

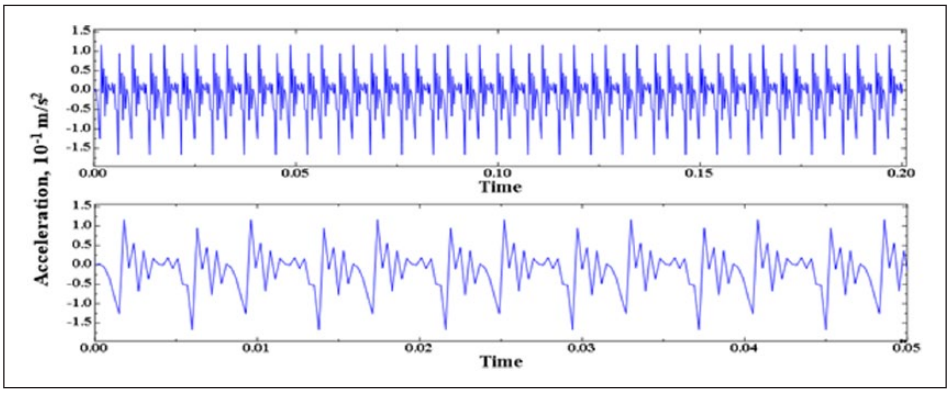

Figure 17. Numerical acceleration response for bearings with defected outer race at position 1 "θ = 0°—defect is located at the load zone".

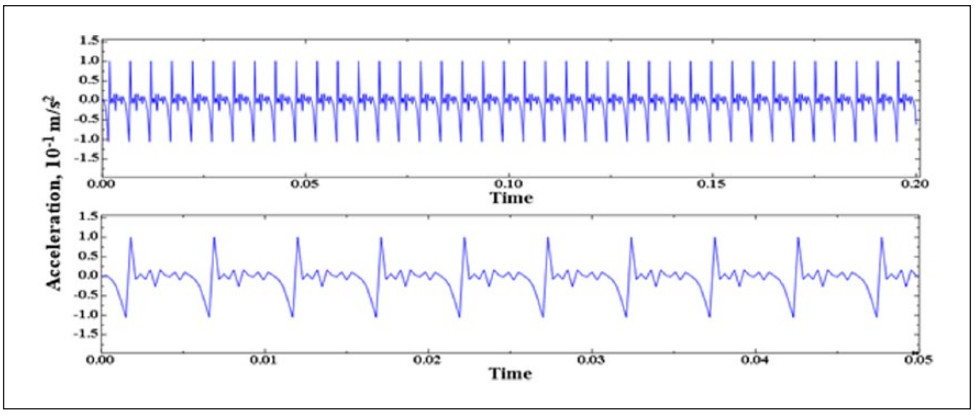

Figure 18. Numerical acceleration response for bearings with defected outer race at position 3 "θ = 180°—defect is located at the unload zone".

signals without using a technique based on wavelet packet analysis.

By calculating the value of vibration impact duration Δt for the same defect with different position, it is found that the vibration impact duration values are uneven. It may be due to the value of the contact area between the outer race and the rollers $(2a_\varphi)$ that changes around the loop resulting of the load value. It can be concluded that the mating surface width, which was calculated according to equation (10), does not indicate the value of the defect width, but it is considered that the value of the defect width with adding the value of the contact area. So, the outer-race defect width may be calculated according to the following equation

$$t = \begin{cases} b - 2a_\varphi & \text{when ball passes} \\ & \text{through load area} \\ b & \text{eleswhere} \end{cases} \quad (12)$$

where half-width of the contact area between the outer race and the rollers (a_φ) is calculated according to the following equation

$$a_\varphi = a\left[1 - \frac{1}{2\varepsilon}(1 - \cos\varphi)\right]^{1.11} \quad (13)$$

The previous results show that both the defect size and defect position play an important role in the value of the vibrations generated. The operating conditions also have a clear effect on the value of the vibration response. Based on that, the contact area values are calculated around the inner surface of the outer race, through which the effect of the different types of bearing installation on the generated stresses and the bearing life. Figure 19 illustrate the relationship between the half-width a of the rectangular contact area versus the angular extent of the load zone. It may be noticed that the maximum value of the contact area at the angle of 0°, at the center of the race, which has

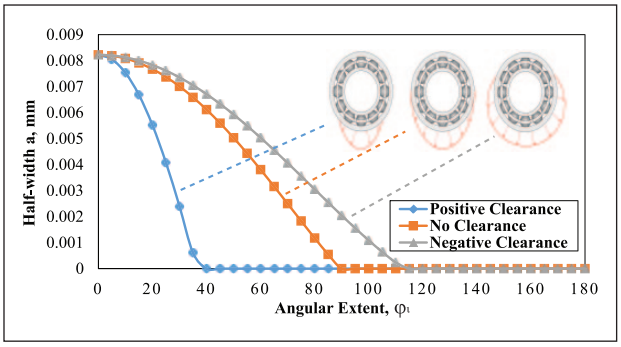

Figure 19. Contact area versus the angular extent of the load zone.

the greatest load value. And the contact area shall be equal to 0 in the no-load zone. It can be observed that the negative clearance, the loading zone is larger so that the contact areas between the rollers and the outer-race extent on a large part of the loop. It can be concluded that the value of the hertz contact area between the roller and the race depends on the bearing installation.

The RMS of the acceleration response calculated for healthy and defected bearings versus rotational speed for the different defect size at the same radial force of 200 N is displayed in Figure 20. The investigation of the bearing behavior has been carried out for bearing with load distribution factor "ε" of 0.5, which means bearing with zero clearance. It can be seen from Figure 20 that the RMS increases with the increase in defect size. The same observation is valid for the acceleration response verses radial load for the different defect size at the same shaft speed of 1000 r/min, as illustrated in Figure 21. It can be concluded that the defect size has a great impact on the generated vibrations. It may be attributed to the fact that increasing the defect size leads to the increase of contact time between the defected area and the outer race. The defect positions of the outer race changes to have locations at 0°, 45°, and 180°. The effect of the defect positions on the acceleration

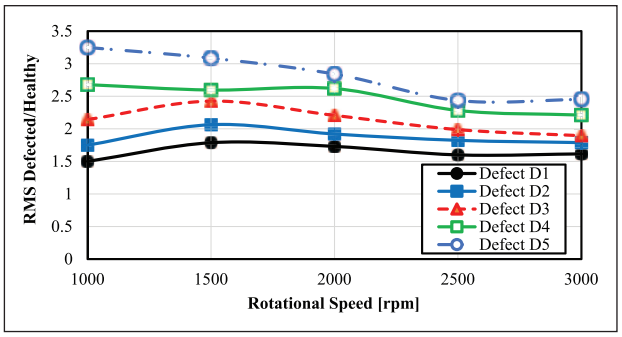

Figure 20. Acceleration response versus shaft speed for different defect size at constant radial load "200 N".

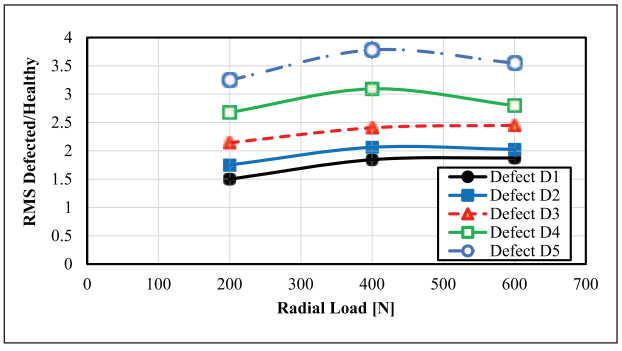

Figure 21. Acceleration response versus radial load for different defect size at constant shaft speed "1000 r/min".

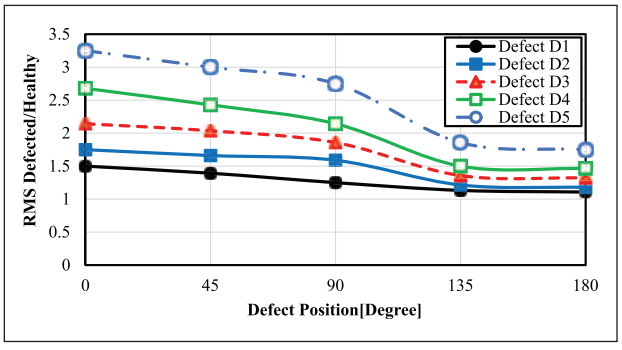

Figure 22. Acceleration response versus defect position for different defect sizes.

response RMS for a bearing with zero clearance is illustrated in Figure 22. It is clear that, the positioning of the outer-race defect affects significantly the intensity of the generated vibration. Furthermore, it is noticed that RMS at the defect positions 0° and 45° have its greater values than for the defect position 180°, which means that the intensity of the generated vibration takes its greatest values at the loading zone "i.e. contact zone" between the rollers and the race.

Figure 23 displays the effect of different types of bearing setting on the value of vibration signals for the defected

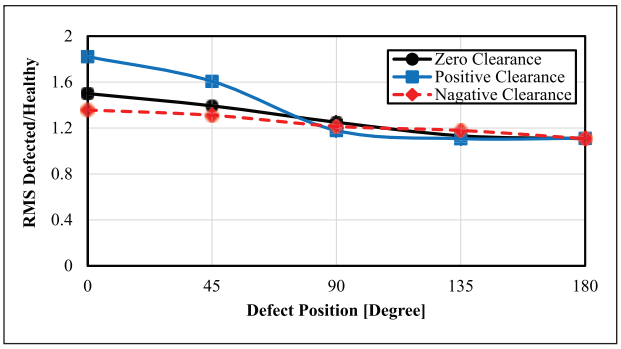

Figure 23. Acceleration response for three primary conditions of bearing setting.

bearing which has 0.46 mm width at the constant rotational speed and radial load. It can be observed that the RMS value for acceleration with positive clearance, $\varepsilon = 0.3$, gives the high result at 0° defect position. However, RMS value of the negative clearance, $\varepsilon = 0.75$, for the same position has the lowest value. It may be due to the fact that not only the defect size and its position are the effects on the value of vibration signals but also the type of bearing setting according to the equation (8). Furthermore, the acceleration response of the defected and healthy bearings is almost constant for different types of bearing settings at 180° defect position. It can be concluded that the defects located at the radial-load distribution area have more effect than the defects located at the unloaded area.

Conclusion

In this study, a numeric model of tapered rolling bearing using ABAQUS/CAE is developed. Based on the results from the experimental setup and the numeric model, it was noticed that a good agreement between the simulation and experimental results during the action of the bearing dynamic load was achieved. The variation between the experimental and simulation results is less than 4.8%. The investigation of the bearing behavior has been carried out for three primary conditions of bearing setting, which are positive, negative, and zero clearance. The outer race is installed in five different positions such that the defect located at 0°, 45°, 90°, 135°, and 180°. The vibration signal pattern obtained from the simulation was found to have similar characteristics with experimental data. It can be concluded that defect-size estimation is more precise when the defect is introduced in the unloading area, where the contact time depends directly on the size of the defect, through which it is easy to calculate the defect value.

Acknowledgements

The authors are would like to express their gratitude to Prof. Dr Mohamed Aly Omar Mousa.

Declaration of conflicting interests

The author(s) declared no potential conflicts of interest with respect to the research, authorship, and/or publication of this article.

Funding

The author(s) received no financial support for the research, authorship, and/or publication of this article.

ORCID iD

Ahmed Nabhan https://orcid.org/0000-0001-7841-1115

References

1. Tandon N and Choudhury A. A review of vibration and acoustic measurement methods for the detection of defects in rolling element bearings. *Tribol Int* 1999; 32(8): 469–480.
2. Gupta P and Pradhan MK. Fault detection analysis in rolling element bearing: a review. *Mater Today: Proc* 2017; 4: 2085–2094.
3. Ocak H and Loparo KA. Estimation of the running speed and bearing defect frequencies of an induction motor from vibration data. *Mech Syst Signal Pr* 2004; 18: 515–533.
4. Kiral Z. *Simulation and analysis of vibration signals generated by rolling element bearings with defects*. PhD Thesis, The University of Izmir, Izmir, 2002.
5. Kiral Z and Karagulle H. Simulation and analysis of vibration signals generated by rolling element bearing with defects. *Tribol Int* 2003; 36: 667–678.
6. Nabhan A, Nouby M, Samy AM, et al. Vibration analysis of deep groove ball bearing with outer race defect using ABAQUS. *J Low Freq Noise V A* 2016; 35(4): 312–325.
7. Nabhan A, Nouby M, Samy AM, et al. Multiple defects detection in outer race of gearbox ball bearing using time domain statistical parameters. *Int J Veh Struct Syst* 2016; 8(3): 167–174.
8. Karacay T and Akturk N. Experimental diagnostics of ball bearings using statistical and spectral methods. *Tribol Int* 2009; 42: 836–843.
9. Al-Dossary S, Raja Hamzah RI and Mba D. Observations of changes in acoustic emission waveform for varying seeded defect sizes in a rolling element bearing. *Appl Acoust* 2009; 70: 58–81.
10. Zhang S, He Q, Ouyang K, et al. Multi-bearing weak defect detection for wayside acoustic diagnosis based on a time-varying spatial filtering rearrangement. *Mech Syst Signal Pr* 2018; 100: 224–241.
11. Hemmati F, Orfali W and Gadala MS. Roller bearing acoustic signature extraction by wavelet packet transform, applications in fault detection and size estimation. *Appl Acoust* 2016; 104: 101–118.
12. Ahmadi AM and Howard CQ. A defect size estimation method based on operational speed and path of rolling elements in defective bearings. *J Sound Vib* 2016; 385: 138–148.
13. Patel VN, Tandon N and Pandey RK. Vibration studies of dynamically loaded deep groove ball bearings in presence of local defects on races. *Procedia Engineer* 2013; 64: 1582–1591.
14. Mishra C, Samantaray AK and Chakraborty G. Bond graph modeling and experimental verification of a novel scheme for fault diagnosis of rolling element bearings in special operating conditions. *J Sound Vib* 2016; 377: 302–320.
15. Mishra C, Samantaray AK and Chakraborty G. Ball bearing defect models: a study of simulated and experimental fault signatures. *J Sound Vib* 2017; 400: 86–112.
16. Neisi N, Sikanen E, Heikkinen JE, et al. Effect of off-sized balls on contact stresses in a touchdown bearing. *Tribol Int* 2018; 120: 340–349.
17. Chen A and Kurfess TR. A new model for rolling element bearing defect size estimation. *Measurement* 2018; 114: 144–149.
18. Bourbatache K, Guessasma M, Bellenger E, et al. DEM ball bearing model and defect diagnosis by electrical measurement. *Mech Syst Signal Pr* 2013; 41: 98–112.
19. Harris TA and Kotzalas MN. *Essential concepts of bearing technology*. 5th ed. Boca Raton, FL: CRC Press, 2006.